

# Detection of the blood hemoglobin using an electro-optical biosensor based on a structurally chiral medium

Nadia Ghorani <sup>a</sup>, Amir Madani<sup>\*a</sup>, Samad Roshan Entezar <sup>b</sup>

*a* Department of Laser and Optical Engineering, University of Bonab, Bonab, Iran  
*b* Faculty of Physics, University of Tabriz, Tabriz, Iran

\* Corresponding Author Email: [a-madani@ubonab.ac.ir](mailto:a-madani@ubonab.ac.ir)

DOI: 10.30495/ijbbe.2023.1998979.1035

## ABSTRACT

Received: Nov. 2, 2023, Revised: Dec. 14, 2023, Accepted: Dec. 24, 2024, Available Online: Jan. 20, 2024

*In this work, a biosensor based on a structurally chiral medium (SCM) under the effect of a low-frequency electric field has been designed to detect blood hemoglobin. The introduced structure is irradiated with a circularly polarized light under an electro-optical Pockels effect. A photonic band gap is observed in the transmission spectrum of the right-handed circularly polarized waves, which indicates the circular Bragg phenomenon. The sample layer is placed between two identical SCMs. The transfer matrix method (TMM) is utilized for the evaluation of the sensor performance. The results show that the defect mode is sensitive to any change in the refractive index of the defect layer where the defect layer is infiltrated with samples with different concentrations of blood hemoglobin. Also, it is shown that applying a low-frequency electric field increases the sensitivity of the mentioned sensor. It is observed that the sensitivity can be expanded up to 142.66 nm/RIU by changing the various parameters of the SCM.*

## KEYWORDS

*Structurally chiral medium, Blood hemoglobin, Circularly polarized light, Photonic band gap, Transfer matrix method, Electro-optical Pockels effect.*

## I. INTRODUCTION

In recent years, structures with alternating refractive indices, called photonic crystals, have attracted much attention in the scientific communities [1,2]. A distinguishing feature of these structures is the photonic bandgap (PBG), which is a range of wavelengths where there is no propagation of electromagnetic waves in the structure [3]. A special type of photonic crystal is a structurally chiral medium (SCM) [4]. These continuous and inhomogeneous media have a gradient spiral refractive index around a

fixed axis. The main feature of these media is the circular Bragg phenomenon (CBP), in which a circularly polarized wave where its handedness matches with the structure's handedness is strongly reflected in a special wavelength region, while a wave with opposite polarization is mainly transmitted [5,6]. Typical examples of such structures are cholesteric liquid crystals and chiral photonic elastomers. Recently, SCMs have found applications in optical sensing to detect chemical, biological, and gaseous samples. SCM-based sensors are compact and have the ability of real-time

monitoring and wide dynamic range. It is possible to adjust the photonic band gap range of these structures by doping them with metal nanoparticles and also by applying an external low-frequency electric field.

Today, diagnosing some diseases such as HIV, cancer and hepatitis is a challenging medical task. In most cases, the diagnosis of these diseases needs accurate blood tests. The dielectric constant of different blood samples with unique compositions is unique and is very useful for disease diagnosis, metabolism regulation, and biochemical analysis [7,8].

Optical biosensors are analytical detectors in which the interactions of blood are converted into an optical signal. In addition, biosensors have many advantages that make them advantageous compared to conventional diagnostic techniques, such as one-step detection and ease of use, which allow for better and faster control of measurements [9]. Many types of biosensors work based on electrical, electromechanical, magnetic, acoustic, and optical mechanisms [10-13]. An optical transducer mechanism is a system that modulates the interaction with optical radiation in a detectable device [9].

In this work, the SCM which is a special photonic structure has been used for sensing. We have developed a highly sensitive optical biosensor based on the defective structure of SCM, which is influenced by the low-frequency electric DC field by the Pockels effect. The transmission of circularly polarized light is calculated using TMM and the effect of different parameters is studied to achieve the highest performance of the sensor configuration. A change in blood hemoglobin concentration causes a significant change in the position of the peak wavelength in the transmission spectrum. Therefore, by observing the transmission spectra of the designed biosensor structure, it is possible to detect different concentrations of blood hemoglobin.

## II. THEORETICAL DESCRIPTION

The chiral medium with the isotropic defect layer of the blood sample is shown in Fig. 1, where  $P$  is the system pitch and  $\chi$  is the tilt angle of the optical axis of the structure. Here, the rotation and heterogeneity of the system are along the  $x$  direction. The incident angle of the electromagnetic wave is  $\theta$ . The structure is between  $x = 0$  to  $x = L$ . The matrix representation of Maxwell's equations in a non-magnetic medium, with 4 components of electric and magnetic fields as  $\varphi(x) = (e_y, e_z, h_y, h_z)$  is [3]:

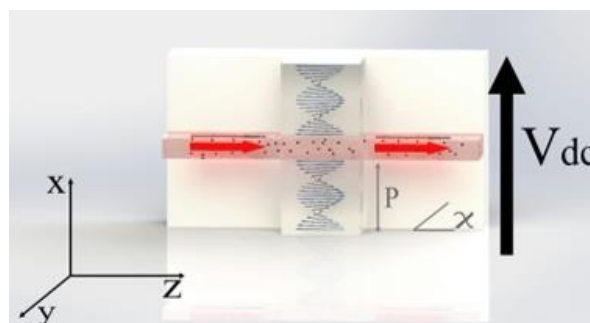


**Fig. 1** Schematic diagram of the designed SCM-based biosensor.  $P$  is the pitch of the SCM and  $\chi$  is the tilt angle of the optical axis of the structure.

$$\frac{d\varphi(x)}{dx} = ik_0 A(x)\varphi_0(x) \quad (1)$$

where  $k_0$  is the wave vector in free space, and the matrix  $A$  is:

$$A(x) = \begin{pmatrix} 0 & 0 & 0 & 1 \\ 0 & 0 & 0 & -1 \\ \frac{\varepsilon_{zx}(x)\varepsilon_{yx}(x)}{\varepsilon_{xx}(x)} - \varepsilon_{zy}(x) & \frac{\varepsilon_{zx}(x)\varepsilon_{xz}(x)}{\varepsilon_{xx}(x)} - \varepsilon_{zz}(x) & 0 & 0 \\ \varepsilon_{yy}(x) - \frac{\varepsilon_{yx}(x)\varepsilon_{xy}(x)}{\varepsilon_{xx}(x)} & \varepsilon_{yz}(x) - \frac{\varepsilon_{yx}(x)\varepsilon_{xz}(x)}{\varepsilon_{xx}(x)} & 0 & 0 \end{pmatrix} + \begin{pmatrix} 0 & 0 & 0 & 1 \\ 0 & 0 & -1 & 0 \\ \frac{\varepsilon_{zx}(x)\varepsilon_{yx}(x)}{\varepsilon_{xx}(x)} & \frac{\varepsilon_{zx}(x)\varepsilon_{xz}(x)}{\varepsilon_{xx}(x)} & 0 & 0 \\ -\frac{\varepsilon_{yx}(x)\varepsilon_{xy}(x)}{\varepsilon_{xx}(x)} & -\frac{\varepsilon_{yx}(x)\varepsilon_{xz}(x)}{\varepsilon_{xx}(x)} & 0 & 0 \end{pmatrix} \quad (2)$$

Here, the elements of the structure's dielectric tensor ( $\varepsilon_{i,j}(x) = (i, j = x, y, z)$ ) under the electric field are

$$\varepsilon = \begin{pmatrix} \varepsilon_1^{(0)} & -r_{63}\varepsilon_1^{(0)}E_3^{dc} & -r_{41}\varepsilon_1^{(0)}E_2^{dc} \\ -r_{63}\varepsilon_1^{(0)}E_3^{dc} & \varepsilon_1^{(0)} & -r_{41}\varepsilon_1^{(0)}E_1^{dc} \\ -r_{41}\varepsilon_3^{(0)}E_2^{dc} & -r_{41}\varepsilon_1^{(0)}E_3^{dc} & \varepsilon_3^{(0)} \end{pmatrix} \quad (3)$$

Here,  $E_K^{dc}$  ( $K=1,2,3$ ) represents the dc electric field components in the principal coordinate system,  $\varepsilon_1^{(0)}, \varepsilon_2^{(0)}, \varepsilon_3^{(0)}$  are the elements of the dielectric tensor in the principal coordinate system, and  $r_{jk}$  ( $1 \leq j \leq 6$  and  $1 \leq K \leq 3$ ) are the electro-optic coefficients.

Using boundary conditions and the TMM, the reflection and transmission coefficients are calculated as [5]

$$\begin{bmatrix} t_R \\ t_L \\ r_R \\ r_L \end{bmatrix} = \begin{bmatrix} t_{RR} & t_{RL} \\ t_{LR} & t_{LL} \\ r_{RR} & r_{RL} \\ r_{LR} & r_{LL} \end{bmatrix} \begin{pmatrix} a_R \\ a_L \end{pmatrix} \quad (4)$$

### III. RESULTS AND DISCUSSION

For the chiral structure in the absence of a defect layer (air/SCM/air), the dielectric permittivity of the chiral material is considered to be  $\varepsilon_1 = 2.7$  and  $\varepsilon_3 = 3.2$ . Also,  $L = 20p$  where the pitch of the structure is  $p = 360nm$  [4,6]. First, the reflection and transmission spectra are represented as a function of the wavelength in Fig 2. Here, Fig. 2(a) and Fig. 2(b) show the right-handed co-polarized transmission and reflection of the structure with a circular Bragg PBG in the visible range. This PBG is due to the chirality of the structure with tilt angle  $\chi = \frac{\pi}{4}$

represents the reduced transmission and increased reflection for a right-handed light at an incident angle of  $\theta = 0^\circ$ . It should be noted that this PBG is highly sensitive to the characteristics of the chiral medium. As the figure shows, applying an electric field to the structure and increasing it increases the width of the band gap. Fig. 2(c) and (d) represent the left-handed co-polarized transmission and reflection of the structure. Here, we see the co-polarized spectra of the system do not contain any PBG for the left-handed light. Also, Fig. 2(e) and (f) show the cross-polarized transmission and reflection.

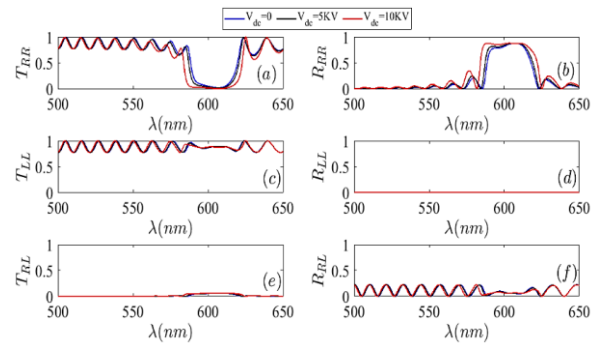


**Fig. 2** Transmission and reflection spectra of the designed structure (air/SCM)/air) as a function of wavelength, with  $\chi = \frac{\pi}{4}$ ,  $\theta = 0^\circ$ , and  $p = 360nm$  in the absence of the defect layer and the effect of different voltages of 0 KV, 5 KV, and 10 KV.

In Fig.3, we plotted the transmission and reflection spectra of the defective system with the structure (air/SCM/defect/SCM/air) at normal incidence of light  $\theta = 0^\circ$ . Here, the

thickness and the refractive index of the defect layer are 700 nm and  $n_s=1$ , respectively. The thickness of SCMs is  $L = 10P$  with  $p = 360\text{nm}$ ,  $\varepsilon_1 = 2.7$ ,  $\varepsilon_3 = 3.2$ , and the tilt angle of  $\chi = \frac{\pi}{4}$ . Also, the other characteristics of the chiral medium are the same as those described in Fig. 2. The results show a defect mode inside the circular PBG. The wavelength and transmittance of the resonant mode depend on the applied voltage. It is clear from the figures that the electric field shifts the resonance to the shorter wavelengths.

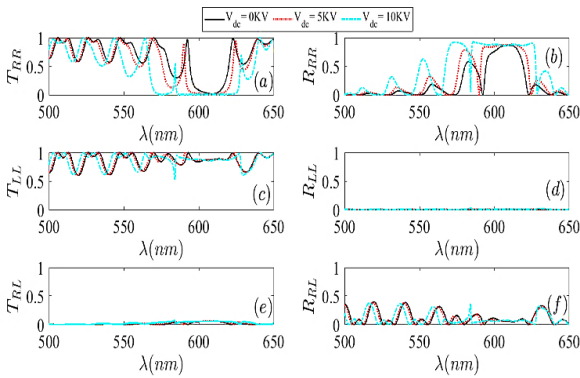


**Fig.3** Transmission and reflection spectra of the defective structure (air/SCM/air/SCM/air), as a function of wavelength, with  $\chi = \frac{\pi}{4}$ ,  $\theta = 0^\circ$ , and  $p = 360\text{nm}$  for different voltages of 0 KV, 5 KV, and 10 KV.

### The sensitivity of the sensor

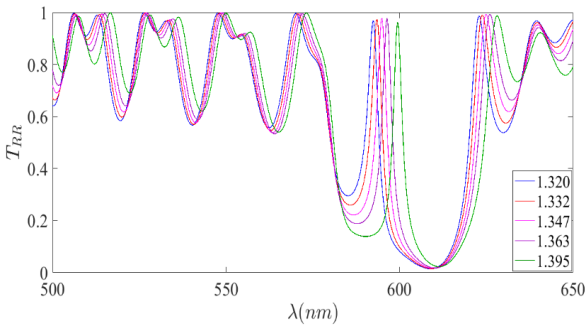


**Fig.4** Transmission spectrum of the sensor for different concentrations of blood hemoglobin with  $d_d = 700\text{ nm}$  and  $\theta = 0^\circ$  and  $\chi = \frac{\pi}{4}$ .

Now, the proposed sensor with the structure air/SCM/defect/SCM/air is used to detect different blood samples. Here, we assume that  $\chi = \frac{\pi}{4}$ ,  $d_d=700\text{ nm}$ , and  $\theta = 0^\circ$ . In Fig. 4, we

represent the transmission spectra of the sensor for the blood samples with different hemoglobin concentrations and therefore different refractive indices. It is evident from the figure that the increase in the refractive index of the defect layer results in a redshift of the defect mode's wavelength. For example, the 5th sample has the largest value of the refractive index and the defect mode appeared at the longest wavelength. Therefore, by calibrating this system, it can be used as a biosensor. So, the blood hemoglobin concentration can be determined by obtaining the wavelength of the defect mode.

We use the figure of merit, FOM, to determine the accuracy and resolution of the designed sensor:

$$FOM = \frac{S}{FWHM} \quad (6)$$

Here, FWHM is the full width at half-maximum, and  $S$  is the sensitivity of the sensor, which is defined as:

$$S = \frac{\Delta\lambda_d}{\Delta n_s} \quad (5)$$

where  $\lambda_d$  shows the wavelength of the defect mode. Also, we use the quality factor,  $Q$ , as a parameter to determine the capability of the proposed sensor to detect biological factors such as blood sample

$$Q = \frac{\lambda_d}{FWHM} \quad (7)$$

The detection limit  $\delta$  which is the maximum acceptable performance of the proposed optical biosensor, is defined as follows:

$$\delta = \frac{FWHM}{S} \quad (8)$$

Table 1 summarizes the results for the different concentrations of blood hemoglobin for two values of the applied voltage. The calculated sensitivity describes the proposed sensor's potential applications for different concentrations of blood hemoglobin detection with high sensitivity. Also, it is clear that the performance of the sensor depends strongly on the applied voltage.

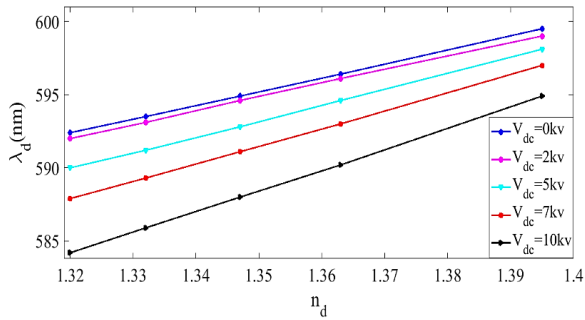


Fig. 5 The variation of the wavelength of the defect mode ( $\lambda_d$ ) versus the refractive index of the defect layer.

In Fig. 5, the variation of the wavelength of the defect mode ( $\lambda_d$ ) versus the refractive index of the defect layer is depicted. As the blood hemoglobin concentration increases,  $\lambda_d$  experiences a redshift because of the change in the refractive index of the blood sample. We can see the effect of different voltages on the designed biosensor in Fig. 5. As it is evident from the figure, the increase in the voltage increases the slope of the graph which means an increase in the sensitivity of the sensor. Various data of the sensor under the effect of DC voltage can be seen in Table 1. These data verify the results of Fig. 5 and show the improvement of the sensor's performance by the increase of the voltage.

Table 1 The sensitivity, Q-factor, limit of detection, and FOM of the proposed sensor for different concentrations of blood hemoglobin and keeping  $d_d = 700$  nm,  $\chi = \frac{\pi}{4}$ . The applied voltage is  $V_{DC}=0$  in part 1 and  $V_{DC}=10KV$  in part 2. [14].

0KV

Blood sample concentration	Refractive index ( $n_s$ )	Sensitivity ( $\frac{nm}{RIU}$ )	Q-factor	$\delta$	$FOM(\frac{1}{RIU})$
0g/L	1.320	-	134.63	-	-
4.6g/L	1.332	91.66	144.75	0.04	22.35
10.4g/L	1.347	92.59	148.72	0.04	23.13
16.5g/L	1.363	93.02	161.18	0.03	25.14
28.7g/L	1.395	94.66	187.34	0.03	29.58

10KV

Blood sample concentration	Refractive index ( $n_s$ )	Sensitivity ( $\frac{nm}{RIU}$ )	Q-factor	$\delta$	$FOM(\frac{1}{RIU})$
0g/L	1.320	-	649.11	-	-
4.6g/L	1.332	141.66	732.37	0.005	177.7

10.4g/L	1.347	140.74	735	0.005	175.09
16.5g/L	1.363	139.53	843.14	0.005	199.32
28.7g/L	1.395	142.66	991.5	0.004	237.76

The effect of the sample's thickness

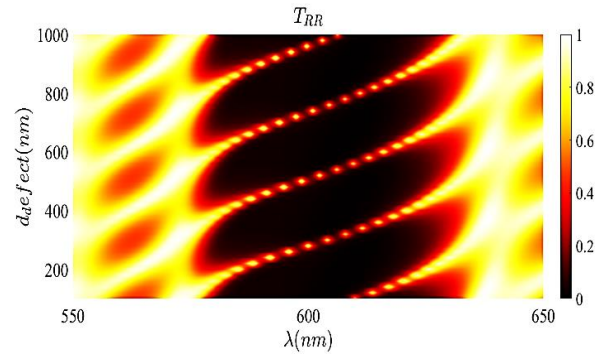


Fig. 6 Transmission spectra of the defected SCM as a function of the incident light wavelength and the sample's thickness layer with  $\chi = \frac{\pi}{4}$ ,  $\theta = 0^\circ$ ,  $p = 360nm$ , and  $n_s = 1$  for  $V_{DC}=5KV$ .

In this part, the effect of the sample's thickness is investigated. It can be observed from Fig. 6 that the change of the sample's thickness within the structure from 100 nm to 900 nm results in a redshift of the defect mode. Besides, the mean sensitivity and other performance parameters of the sensor based on the different thicknesses of the sample can be observed in Table 2 in which the applied voltage is considered as  $V_{DC}=5KV$ . The increase in the thickness of the sample improves the performance of the sensor.

Table 2 The mean sensitivity, Q-factor, limit of detection, and FOM of the proposed sensor for different concentrations of blood hemoglobin and different sample thicknesses with  $\chi = \frac{\pi}{4}$ ,  $\theta = 0^\circ$ ,  $V_{DC}=5KV$ .

Thickness	Sensitivity ( $\frac{nm}{RIU}$ )	Q-factor	$\delta$	$FOM(\frac{1}{RIU})$
100nm	12.93	258.66	0.1	5.47
200nm	27.54	196.51	0.1	9.24
300nm	36.05	275.17	0.05	16.68
400nm	39.56	217.7	0.06	14.76
500nm	71.44	345.29	0.02	41.05
600nm	69.86	253.33	0.03	28.63
700nm	91.73	310.82	0.02	47.77

800nm	91.06	276.54	0.02	41.01	16.5g/L	1.363	106.97	396.4	0.01	71.13
900nm	104.68	324.33	0.01	60.78	28.7g/L	1.395	108	398.73	0.01	72

### The effect of the tilt angle of SCM

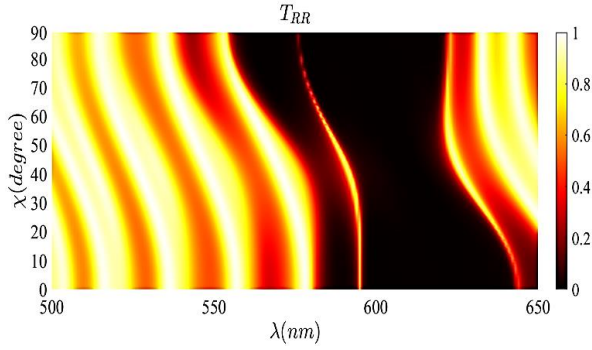


Fig. 7 Transmission spectra of the defected SCM as a function of the incident light wavelength and tilt angle with  $\theta = 0^\circ$ , and  $p = 360nm$ ,  $d_d = 700nm$ ,  $n_s = 1$  where  $V_{DC}=5$  KV.

Here, the influence of the tilt angle of the SCM on the performance of the designed sensor will be investigated for  $V_{DC}=5KV$ . Fig.7 illustrates the transmission of the sensor for different tilt angles. At a certain sample's thickness,  $d=700nm$ , it is evident that the increase of the tilt angle has a remarkable effect on the bandwidth of the PBG and the transmittance of the defect mode where the maximum value of the transmittance is obtained for  $\chi = \frac{\pi}{4}$ . The sensitivity and other parameters of the sensor based on the different tilt angles of the SCM are summarized in Table 3 for  $V_{DC}=5KV$ . The results confirm that the increase of the tilt angle to the larger values has an undesirable effect on the performance of the sensor. According to the obtained data, the highest sensitivity has been obtained at an angle of  $\chi = \frac{\pi}{4}$ .

Table 3 The mean sensitivity, Q-factor, limit of detection, and FOM of the proposed sensor for different concentrations of blood hemoglobin  $\chi = \frac{\pi}{4}$  with  $V_{DC}=5KV$ .

Blood sample concentration	Refractive index ( $n_s$ )	Sensitivity ( $\frac{nm}{RIU}$ )	Q-factor	$\delta$	FOM ( $\frac{1}{RIU}$ )
0g/L	1.320	-	245.83	-	-
4.6g/L	1.332	100	268.72	0.02	45.45
10.4g/L	1.347	103.70	312	0.01	54.57

In Fig. 8 we have plotted the calibration curve of the sensor which shows the sensitivity of the sensor as a function of the applied voltage. The obtained curve represents that the sensitivity increases almost linearly with the increase of the voltage.

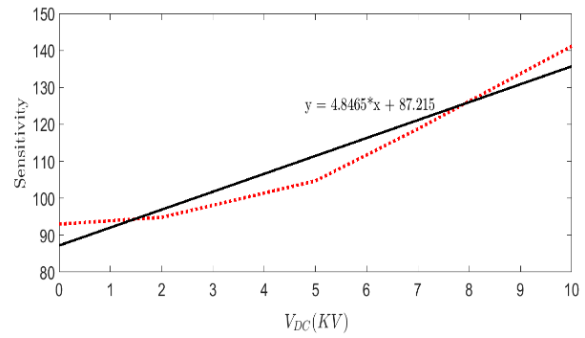


Fig. 8 The calibration curve of the sensor, sensitivity as a function of the applied voltage.

Finally, it should be mentioned that the designed sensor can show the selectivity properties in experimental works. Selectivity is a property of the sensor based on the chemical bonds between the target and the surface of the sensor. However, this bond cannot be checked in theoretical works and only the concentration of the target can be checked.

## IV. CONCLUSION

In this paper, we have developed a theoretical strategy for a sensor by a defective SCM structure under the influence of a low-frequency electric field for the detection of blood hemoglobin. It is shown that the position and transmittance of the defect mode depend on the concentration of the sample and the applied voltage. Also, the sensitivity of the sensor increases with the increase of the voltage. The effect of the thickness of the defect layer and the tilt angle of the chiral medium along with the dc voltage effect on the performance of the proposed sensor have been investigated. It is observed that the increase in the thickness of the sample improves the performance of the sensor while the increase of the tilt angle to the larger

values has an undesirable effect on the performance of the sensor. By changing the concentration of the blood sample, the peak wavelength of the defect mode is shifted toward the longer wavelength. By optimizing various sensor parameters, it was possible to increase the sensitivity of the proposed sensor. DC voltage has a significant effect on increasing the sensitivity of the designed sensor, which can be a suitable option for detecting different blood samples.

## REFERENCES

- [1] A. Lakhtakia and R. Messier, *Sculptured Thin Films: Nanoengineered Morphology and Optics*, 2005.
- [2] J. C. Hernández and J. A. Reyes, "Optical band gap in a cholesteric elastomer doped by metallic nanospheres," *Physical Review E*, vol. 96, pp. 062701 (1-6), 2017.
- [3] J. Mendoza, J. A. Reyes, and C. G. Avendaño, "Optical band gap in a nanocomposite structurally chiral medium," *Physical Review A*, vol. 94, pp. 053839 (1-5), 2016.
- [4] C. G. Avendaño and L. O. Palomares, "Omnidirectional narrow optical filters for circularly polarized light in a nanocomposite structurally chiral medium," *Applied Optics*, vol. 57, pp. 3119-3125, 2018.
- [5] C. G. Avendaño and D. Martínez, "Tunable omni-directional mirror based on one-dimensional photonic structure using twisted nematic liquid crystal: the anchoring effects," *Applied Optics*, vol. 53, pp. 4683-4690, 2014.
- [6] J. A. Reyes and A. Lakhtakia, "Electrically controlled optical band gap in a structurally chiral material," *Optics Communications*, vol. 259, pp. 164-173, 2006.
- [7] H. Inan, M. Poyraz, F. Inci, M. A. Lifson, M. Baday, B. T. Cunningham, and U. Demirci, "Photonic crystals: emerging biosensors and their promise for point-of-care applications," *Chemical Society Reviews*, vol. 46, pp. 366-388, 2017.
- [8] H. Chen, R. Lou, Y. Chen, L. Chen, J. Lu, and Q. Dong, "Photonic crystal materials and their application in biomedicine," *Drug Delivery*, vol. 24, pp. 775-780, 2017.
- [9] S. K. Srivastava, C. J. M. van Rijn, and M. A. Jongsma, "Biosensor-based detection of tuberculosis," *RSC Advances*, vol. 6, pp. 17759-17771, 2016.
- [10] G. Pitruzzello and T. F. Krauss, "Photonic crystal resonances for sensing and imaging," *Journal of Optics*, vol. 20, pp. 073004 (1-25), 2018.
- [11] N. Ghorani, A. Madani, and S. R. Entezar, "Real-time biosensor application of structurally chiral medium for detection and sensing of plasma in human blood," *Physica Scripta*, vol. 98, pp. 055518 (1-11), 2023.
- [12] H. J. El-Khozondar, P. Mahalakshmi, R. J. El-Khozondar, N. R. Ramanujam, I. S. Amiri, and P. Yupapin, "Design of one dimensional refractive index sensor using ternary photonic crystal waveguide for plasma blood samples applications," *Physica E: Low-dimensional Systems and Nanostructures*, vol. 111, pp. 29-36, 2019.
- [13] Z. A. Zaky and A. H. Aly, "Modeling of a biosensor using Tamm resonance excited by graphene," *Applied Optics*, vol. 60pp. 1411-1419, 2021.
- [14] S. E.-S. Abd El-Ghany, W. M. Noum, Z. S. Matar, Z. A. Zaky, and A. H. Aly, "Optimized bio-photonic sensor using 1D-photonic crystals as a blood hemoglobin sensor," *Physica Scripta*, vol. 96, pp. 035501 (1-9), 2020.

**THIS PAGE IS INTENTIONALLY LEFT BLANK.**